D．研究発表

1．論文発表

1. Ishino K, Kato T, Kato M, Shibata T, Watanabe M, Wakabayashi K, Nakagama H, Totsuka Y. Comprehensive DNA adduct analysis reveals pulmonary inflammatory response contributes to genotoxic action of magnetite nanoparticles. Int J Mol Sci. 2015, Feb 4;16(2):3474-92.
2. Komiya M, Fujii G, Miyamoto S, Takahashi M, Ishigamori R, Onuma W, Ishino K, Totsuka Y, Fujimoto K, Mutoh M. Suppressive effects of the NADPH oxidase inhibitor apocynin on intestinal tumorigenesis in obese KK-Ay and Apc mutant Min mice. Cancer Sci. 2015 Aug 27.

2．学会発表

1. 戸塚ゆ加里、中釜　斉：質量分析機器を用いた DNA 付加体の網羅的解析による中国の食道癌発症要因の解明
第４２回日本毒性学会学術大会. 2015 年 7 月
2. Yukari Totsuka, Yingsong Lin, Mamoru Kato, Yasushi Totoki, Tatsuhiro Shibata, Yoshitaka Matsushima, Hitoshi Nakagama : Exploration of cancer etiology using comprehensive DNA adduct analysis (DNA adductome analysis)日本癌学会学術総会. 2015 年 10 月
3. 戸塚ゆ加里：ゲノム解析および DNA 付加体の網羅的解析による発がん要因の探索, 第 44 回日本環境変異原学会. 2015 年 12 月
4. 秋場　望、椎崎一宏、遠藤　治、三牧幸代、土原一哉、中釜　斉、戸塚ゆ加里：職業性胆管癌の候補物質、ジクロロメタン及び 1,2-ジクロロプロパンの変異原性に対するグルタチオン-S-転移酵素の影響、第 44 回日本環境変異原学会. 2015 年 12 月

(発表誌名巻号・頁・発行年等も記入)

E．知的財産権の出願・登録状況
（予定を含む。）

1．特許取得
該当なし

2．実用新案登録
該当なし

3．その他
該当なし

研究成果の刊行に関する一覧表

書籍

著者氏名	論文タイトル名	書籍全体の編集者名	書　籍　名	出版社名	出版地	出版年	ページ
	該当なし						

雑誌

発表者氏名	論文タイトル名	発表誌名	巻号	ページ	出版年
Ishino K, Kato T, Kato M, Shibata T, Watanabe M, Wakabayashi K, Nakagama H, Totsuka Y.	Comprehensive DNA adduct analysis reveals pulmonary inflammatory response contributes to genotoxic action of magnetite nanoparticles.	Int J Mol Sci.	16(2)	3474-92	2015,
Komiya M, Fujii G, Miyamoto S, Takahashi M, Ishigamori R, Onuma W, Ishino K, Totsuka Y, Fujimoto K, Mutoh M.	Suppressive effects of the NADPH oxidase inhibitor apocynin on intestinal tumorigenesis in obese KK-Ay and Apc mutant Min mice.	Cancer Sci.	106(11)	1499-505	2015

別添４

厚生労働科学研究費補助金（食品の安全確保推進研究事業）
分担研究報告書

オルガノイド皮下移植系実験

研究分担者　落合　雅子
国立研究開発法人国立がん研究センター研究所　主任研究員

研究要旨
腫瘍性病変をエンドポイントとするオルガノイド系を用いる食品添加物等の遺伝毒性・発がん性の短期包括的試験法を開発する。正常マウスの各種臓器からオルガノイドを調整し、遺伝的再構成もしくは化学物質に暴露させた後に、ヌードマウス皮下に移植して腫瘍形成能を解析する試験を担当した。
大腸オルガノイドの腫瘍形成能の解析は、LSL*Kras*$^{G12D/+}$マウス由来オルガノイドの場合、*Kras*活性化のみでは皮下での上皮細胞の増殖は認められたが、異型性はなく、*Apc* shRNAを追加導入（*Kras*^{G12D}→sh*Apc*）しても同様であった。*Kras*^{G12D}→sh*Pten* では異型腺管の増殖が認められ、*Kras*^{G12D}→sh*Apc* +sh*p53*もしくは*Kras*^{G12D}→sh*Apc* +sh*Pten* では、がん組織の増殖が認められた。B6由来大腸オルガノイドでは、sh*Apc*のみでは異型性のない上皮細胞の増殖が認められたのみで、sh*Apc*→sh*Pten*、sh*Apc*→sh*Pten* +sh*p53*の場合に、異型腺管の増殖が認められた。膀胱に関しても、遺伝的再構成による発がんへの影響が示唆された。大腸オルガノイドへの腸管発がん物質PhIPの暴露をモデル系として、化学物質のオルガノイドへの細胞毒性の解析には、NADの還元能を指標とした96 well plateベースの細胞生存性測定試験が利用可能であり、化学物質暴露の際の用量設定に有用であることを示した。
各臓器からのオルガノイドの作成、遺伝的再構成による腫瘍形成能の確認、化学物質のオルガノイドへの細胞毒性の解析による用量設定は、試験法開発のための基礎的データとなる。次年度以降は、化学物質、臓器などの種類を増やして解析する予定である。

（具体的かつ詳細に記入すること）

A．研究目的

腫瘍性病変をエンドポイントとするオルガノイド系を用いる食品添加物等の遺伝毒性・発がん性の短期包括的試験法を開発する。正常マウスの各種臓器からオルガノイドを調整し、遺伝的再構成もしくは化学物質に暴露させた後に、ヌードマウス皮下に移植して腫瘍形成能を解析する試験を担当する。

マウス小腸オルガノイドを用いて、レンチウィルスを用いたがん抑制遺伝子shRNAの導入により、遺伝的再構成を行い、ヌードマウス皮下に移植すると腫瘍様組織を形成可能であることは既に報告した（Onuma K et al., PNAS, 2013）。他臓器に関しては、大腸、肺、膀胱等は、オルガノイド系の調整法を確立している。まず、これらのオルガノイドにレンチウィルスを用いた遺伝子導入による遺伝的再構成を行い、ヌードマウス皮下への移植により、腫瘍形成能を確認する。同時に、オルガノイドへの化学物質の暴露方法や用量設定の手法を検討し、遺伝毒性・発がん性の短期包括的試験法の開発のための基礎的データを得る。

B．研究方法

B6マウスもしくは、LSL-*Kras*^{G12D}マウスの大腸及び膀胱からオルガノイドを作成した。図1に大腸及び膀胱オルガノイドの培養像を示す。

大腸に関しては、LSL-*Kras*^{G12D}マウス由来のオルガノイドを用いた場合は、レンチウィルスにより、Cre recombinase遺伝子を導入して*Kras*を活性化した後に、がん抑制遺伝子shRNAを追加導入した。

図1　大腸及び膀胱オルガノイドの培養像

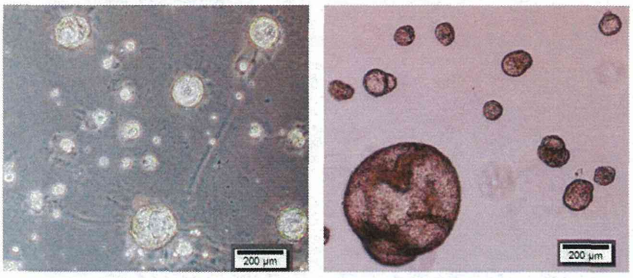

大腸　　膀胱

C57BL6/J(B6)マウス由来大腸オルガノイドの場合は、まず、*Apc* shRNA(sh*Apc*)を導入した後に、他のがん抑制遺伝子shRNAの追加導入を行い、ヌードマウス皮下に移植後、4～6週間で腫瘍形成及び組織型の解析を行った。

膀胱に関しても、B6マウス由来のオルガノイドに、*Pten* shRNAをレンチウィルスで導入し、ヌードマウス皮下に移植後8週間で腫瘍形成及び組織型の解析を行った。

オルガノイドへの化学物質の暴露は、オルガノイドの継代時に行った。オルガノイドの播種から2時間後に、S9 mix（化学物質の代謝活性化のため）存在下、24時間化学物質に暴露させた。暴露終了時に測定試薬を含む培地と交換し、化学物質のオルガノイドに対する細胞毒性を、NADの還元能を指標とした96 well plateベースの細胞生存性測定試験（同じplateを用いて、3日間以上の連続した解析が可能）

を用いて解析した。

C．研究結果

ヒト腸管発がんでは、大部分は大腸に腫瘍が発生するので、小腸のみならず、大腸由来のオルガノイドが利用可能かという点は非常に重要である。そこで、マウス正常大腸由来のオルガノイドに関して、腫瘍形成能を有するか否かを、遺伝的再構成による発がんから解析した。LSL*Kras*$^{G12D/+}$マウス由来大腸オルガノイドの場合、*Kras*活性化のみでは皮下での上皮細胞の増殖は認められたが、異型性はなく、*Apc* shRNAを追加導入（*Kras*^{G12D}→sh*Apc*）しても同様であった。*Kras*^{G12D}→sh*Pten* では異型腺管の増殖が認められ、*Kras*^{G12D} → sh*Apc* +sh*p53* もしくは *Kras*^{G12D} → sh*Apc* +sh*Pten* では、がん組織の増殖が認められた。ヌードマウス皮下腫瘍のマクロ像（図2a）と組織写真（図2b）を示す。

図2a LSL*Kras*$^{G12D/+}$マウス由来大腸オルガノイドの遺伝的再構成- ヌードマウス皮下腫瘍のマクロ像

1　　2

1：*Kras*^{G12D}→shLuc

2：*Kras*^{G12D}→sh*Apc* +sh*p53*

図2b:組織写真（上段1、下段２）

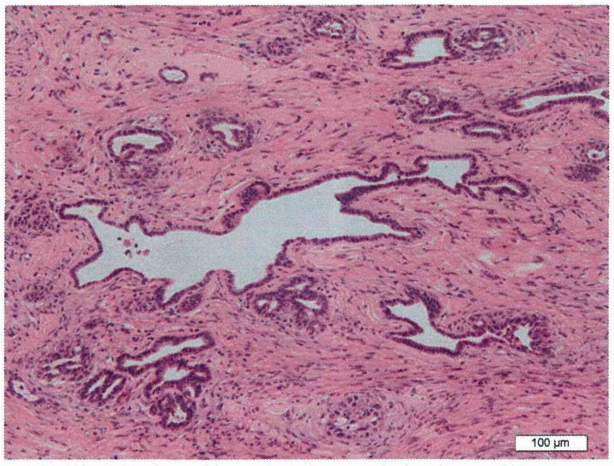

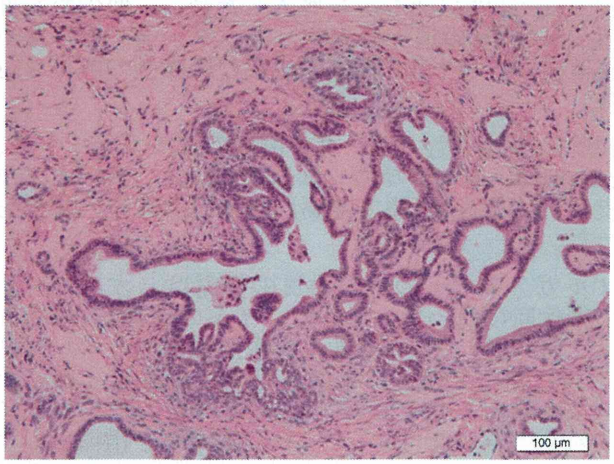

B6由来大腸オルガノイドでは、sh*Apc*のみでは異型性のない上皮細胞の増殖が認められたのみで、sh*Apc*→sh*Pten*、sh*Apc*→sh*Pten* +sh*p53*の場合に、異型腺管の増殖が認められた。図3にヌードマウス皮下腫瘍の組織写真を示す。表1に小腸オルガノイドを用いた場合の遺伝的再構成による発がんの結果との比較を示す。例えば、小腸オルガノイドの場合には、B6でのsh*Apc*のみで異型腺管の増殖が認められる場合があるが、大腸オルガノイドでは、MOCKの場合と組織型は変わらず、大腸オルガノイドの方が腫瘍形成には、より多くの遺伝子変化を必要とする傾向が認められた。*Apc*^{Min}マウス（Apc変異を片方のアレルに持つ）での、腸管の自然発生腫瘍の発生個数が小腸に非常に多く、大腸では極く少ないこととも一致する。また、大腸オルガノイドでも、*Kras*活性化に加えてsh*Apc*の導入、更にsh*p53*もしくはsh*Pten*を導入すれば、がん組織の増殖が認められたので、腫瘍形成能を有することが証明された。

表1　マウス正常小腸/大腸由来オルガノイドの遺伝的再構成による発がん

Mouse	遺伝的再構成	小腸*1,2	大腸*2
B6	MOCK	－～±	－～±
B6	sh*Apc*	±～＋	－～±
B6	sh*p53*	NT	－～±
B6	sh*Pten*	－～±	±
B6	sh*p53* + sh*Pten*	－～±	±
B6	sh*Apc* → sh*p53*	＋＋	－～±
B6	sh*Apc* → sh*Pten*	＋＋	＋
B6	sh*Apc* → sh*p53* + sh*Pten*	＋＋	＋
Kras$^{LSL-G12D/+}$	MOCK	－～±	－～±
Kras$^{LSL-G12D/+}$	Cre	±～＋	±
Kras$^{LSL-G12D/+}$	Cre → sh*Apc*	＋＋	±
Kras$^{LSL-G12D/+}$	Cre → sh*p53*	NT	±
Kras$^{LSL-G12D/+}$	Cre → sh*Pten*	NT	＋
Kras$^{LSL-G12D/+}$	Cre → sh*Apc* + sh*p53*	NT	＋＋
Kras$^{LSL-G12D/+}$	Cre → sh*Apc* + sh*Pten*	NT	＋＋

*1 Onuma K et al., PNAS, 2013より

*2 組織型

－　；　No cells/organoids retention
±；　Proliferated glands without atypia
＋；　Dysplasia
＋＋；　Carcinoma
NT；　Not tested

膀胱に関しても、B6マウスからオルガノイドを作成することが可能であるが、ヌードマウス皮下に移

植した場合には、MOCKを導入しただけのオルガノイドの場合には、上皮細胞が若干認められたのみであった。*Pten* shRNAを導入したオルガノイドでは、腺管が大きくなるなどの細胞増殖への影響が認められ、遺伝的再構成による発がんへの影響が示唆された。

図3：B6由来大腸オルガノイドの遺伝的再構成- ヌードマウス皮下腫瘍の組織写真

sh*Apc*→sh*Luc*

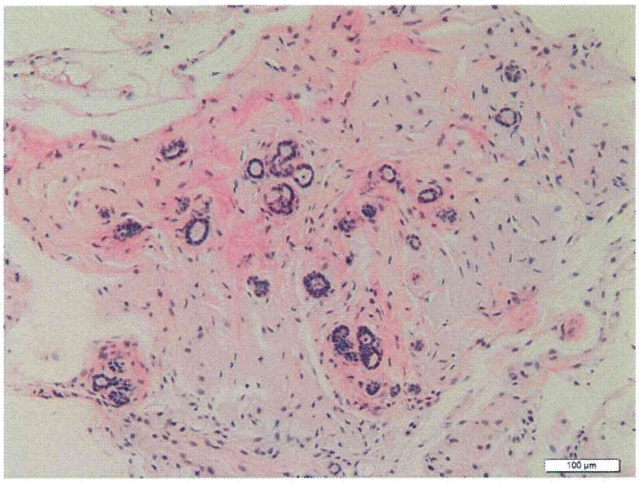

sh*Apc*→sh*p53*+sh*Pten*

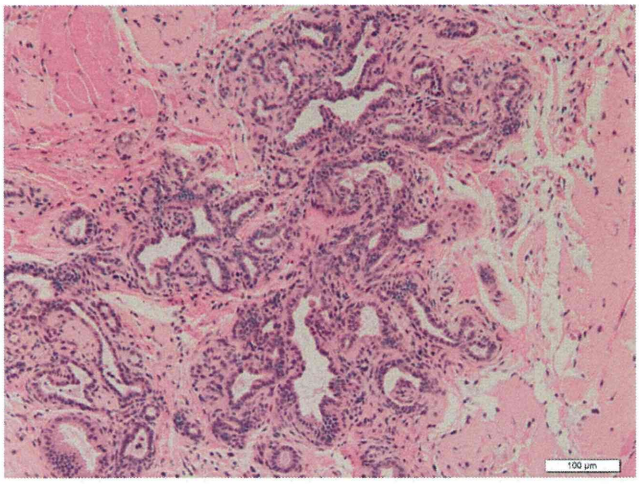

化学物質のオルガノイドに対する細胞毒性の解析に関しては、齧歯類において、腸管への発がん性が報告されているPhIPをモデル化合物として用いて、大腸オルガノイドに暴露させる系において解析した。1 well当たり5000～10000個の細胞数を播種した場合に、NADの還元能を指標とする細胞生存性測定試験において、細胞数に応じた増殖曲線を示し、この試験が、細胞増殖を反映していることが示された。PhIPを0.05~10μMの濃度で(S9mix存在下)、24時間暴露し、暴露終了時点から72時間まで測定した。72時間の時点で、0μMに比して、1μMまでは差が認められず、2～10μMで約９割の細胞生存であったが、細胞増殖の停止などは認められなかった。PhIPが、用量依存性に細胞生存性に影響を与えることが示され、化学物質の暴露の際の用量設定の基礎的データとなることが示された。今後、細胞生存性測定試験でのどのポイント(0μMに比して8~9割の細胞生存か、細胞増殖の停止が誘発される用量か等)を最大用量とするかは、複数回暴露を行い、腫瘍形成能を解析した結果と比較して検討を行う必要がある。大腸オルガノイドを用いた解析結果を示したが、どの臓器由来のオルガノイドにもこの解析法は応用可能である。

各臓器からのオルガノイドの作成、遺伝的再構成による腫瘍形成能の確認、化学物質のオルガノイドへの細胞毒性の解析による用量設定は、試験法開発のための基礎的データとなる。次年度以降は、化学物質、臓器などの種類も増やして解析する予定である。

（倫理面への配慮）
動物実験の実施に際しては、各研究施設の動物実験倫理委員会の承認を得た後に行い、実験動物に対する動物愛護に関して十分配慮して行った。遺伝子組換え生物等を用いる実験については、実施機関の承認を得た。

D．研究発表

1．　論文発表
なし

2．　学会発表
1. 落合 雅子、松浦 哲也、中釜 斉、筆宝 義隆、今井 俊夫。正常上皮細胞の3次元培養による*in vitro*発がんモデルの開発 －化学発がん・予防研究への応用に向けて、がん予防学術大会2015さいたま、さいたま、2015年6月。
2. 落合 雅子、松浦 哲也、中釜 斉、筆宝 義隆、今井 俊夫。マウス正常腸管上皮の３次元培養法を用いる発がん再構成系に対するPhIPの修飾作用、第30回発癌病理研究会、小豆島、2015年8月。
3. 落合 雅子、松浦 哲也、中釜 斉、筆宝 義隆、今井 俊夫。マウス正常腸管上皮の３次元培養法を用いる発がん再構成系に対するPhIPの修飾作用、第74回日本癌学会学術総会、名古屋、2015年10月。
4. 落合 雅子、中釜 斉。マウス正常上皮細胞の３次元培養法を用いる*in vitro*発がんモデルの開発、日本環境変異原学会第44回大会、福岡、2015年11月。

(発表誌名巻号・頁・発行年等も記入)

E．知的財産権の出願・登録状況
（予定を含む。）

1．特許取得
なし

2．実用新案登録
なし

3．その他
なし

別添５

研究成果の刊行に関する一覧表

書籍

著者氏名	論文タイトル名	書籍全体の編集者名	書　籍　名	出版社名	出版地	出版年	ページ
	該当なし。						

雑誌

発表者氏名	論文タイトル名	発表誌名	巻号	ページ	出版年
Maru Y, Orihashi K, Hippo Y	Lentivirus-based stable gene delivery into intestinal organoids.	Methods Mol Biol	in press		
Ishino K, Kato T, Kato M, Shibata T, Watanabe M, Wakabayashi K, Nakagama H, Totsuka Y	Comprehensive DNA adduct analysis reveals pulmonary inflammatory response contributes to genotoxic action of magnetite nanoparticles.	Int J Mol Sci	16 (2)	3474-92	2015,
Komiya M, Fujii G, Miyamoto S, Takahashi M, Ishigamori R, Onuma W, Ishino K, Totsuka Y, Fujimoto K, Mutoh M	Suppressive effects of the NADPH oxidase inhibitor apocynin on intestinal tumori-genesis in obese KK-Ay and Apc mutant Min mice.	Cancer Sci	106 (11)	1499-505	2015

Int. J. Mol. Sci. **2015**, *16*, 3474-3492; doi:10.3390/ijms16023474

OPEN ACCESS
International Journal of
Molecular Sciences
ISSN 1422-0067
www.mdpi.com/journal/ijms

Article

Comprehensive DNA Adduct Analysis Reveals Pulmonary Inflammatory Response Contributes to Genotoxic Action of Magnetite Nanoparticles

Kousuke Ishino [1], Tatsuya Kato [1], Mamoru Kato [2], Tatsuhiro Shibata [2], Masatoshi Watanabe [3], Keiji Wakabayashi [4], Hitoshi Nakagama [1] and Yukari Totsuka [1,*]

[1] Division of Carcinogenesis and Prevention, National Cancer Center Research Institute, 1-1 Tsukiji 5-chome, Chuo-ku, Tokyo 104-0045, Japan; E-Mails: kishino@ncc.go.jp (K.I.); takatou1311@gmail.com (T.K.); hnakagam@ncc.go.jp (H.N.)

[2] Division of Cancer Genomics, National Cancer Center Research Institute, 1-1 Tsukiji 5-chome, Chuo-ku, Tokyo 104-0045, Japan; E-Mails: mamkato@ncc.go.jp (M.K.); tashibat@ncc.go.jp (T.S.)

[3] Division of Materials Science and Engineering, Graduate School of Engineering, Yokohama National University, Hodogaya-ku, Yokohama 240-8501, Japan; E-Mail: mawata@ynu.ac.jp

[4] Graduate Division of Nutritional and Environmental Sciences, University of Shizuoka, 52-1, Yada, Shizuoka 422-8526, Japan; E-Mail: kwakabayashi@u-shizuoka-ken.ac.jp

* Author to whom correspondence should be addressed; E-Mail: ytotsuka@ncc.go.jp; Tel.: +81-3-3542-2511 (ext. 4552); Fax: +81-3-3542-2530.

Academic Editor: James C. Bonner

Received: 11 October 2014 / Accepted: 30 January 2015 / Published: 4 February 2015

Abstract: Nanosized-magnetite (MGT) is widely utilized in medicinal and industrial fields; however, its toxicological properties are not well documented. In our previous report, MGT showed genotoxicity in both *in vitro* and *in vivo* assay systems, and it was suggested that inflammatory responses exist behind the genotoxicity. To further clarify mechanisms underlying the genotoxicity, a comprehensive DNA adduct (DNA adductome) analysis was conducted using DNA samples derived from the lungs of mice exposed to MGT. In total, 30 and 42 types of DNA adducts were detected in the vehicle control and MGT-treated groups, respectively. Principal component analysis (PCA) against a subset of DNA adducts was applied and several adducts, which are deduced to be formed by inflammation or oxidative stress, as the case of etheno-deoxycytidine (εdC), revealed higher contributions to MGT exposure. By quantitative-LC-MS/MS analysis, εdC levels

were significantly higher in MGT-treated mice than those of the vehicle control. Taken together with our previous data, it is suggested that inflammatory responses might be involved in the genotoxicity induced by MGT in the lungs of mice.

Keywords: magnetite nanoparticle; pulmonary inflammation; intratracheal instillation; DNA adductome

1. Introduction

Magnetite nanoparticles (MGT) have been widely utilized in medicinal and industrial fields [1]. Moreover, in medical applications, MGTs are widely used for magnetic resonance imaging as a contrast agent based on their good bio-compatibility [2,3]. With increasing utilization of MGT, it has been a concern whether MGTs are safe for humans or not. Hitherto, several reports describing MGT toxicity have been published [4–13], however, there is still controversy over reports regarding toxicity. Most investigations are focused on studying effects of MGTs on *in vitro* cellular viability, morphology and metabolism, or *in vivo* general toxicity on various organs with various administration routes of MGT (intraperitoneal, intratracheal or intravenous injection). Recently, we have reported genotoxic effects of MGTs using *in vitro* and *in vivo* assay systems, and clearly demonstrated that MGTs induce genotoxicity in both cultured mammalian cells and mice lungs instilled intratracheally [14–16]. Based on mutation spectra, histopathological evaluation, and oxidative- and lipid peroxide-related DNA adduct formations, it is suggested that inflammatory responses might contribute to the genotoxicity induced by MGT treatment [16].

It is well known that DNA adducts are considered to be triggers for induction of gene mutations [17–21]. In our previous report, MGT predominantly induced a C to T transition in mouse lungs [16]. Levels of 8-oxo-7,8-dihydro-2'-deoxyguanosine (8-oxodG) and heptano-etheno (Hε)-adducts were also elevated in lungs of mice exposed to MGT [16]. Although Hε-dC induces C to T transitions *in vitro* [22,23], the mechanisms of genotoxicity induced by MGT are not fully explained yet. Global discovery of DNA adducts in target organs would be useful information for exploring the mechanisms of genotoxicity.

Recently, Kanary *et al.* [24,25], established a method consisting of liquid chromatography followed by double tandem mass spectrometry for comprehensive analysis of DNA adducts in human and animal tissues. The basic strategy is designed to detect the neutral loss of a 2'-deoxyribose moiety [M + H; −116] from positively ionized 2'-deoxynucleoside adducts in multiple reaction ion monitoring mode (MRM) transmitting the precursor ion [M + H] ≥ daughter ion [M + H; −116] [24]. Using this method, hundreds of DNA adducts can be detected at once. Based on this strategy, we recently established comprehensive analysis of DNA adducts by using a UPLC-QTOF mass spectrometer. In this method, MS^E analysis was used to detect the neutral loss of a 2'-deoxyribose moiety [M + H; −116.04736]. Using this method, accurate mass values of precursor ions can be obtained, and this is an advantage for identification of chemical structures of DNA adducts. To identify the chemical structures of DNA adducts screened by adductome analysis, we have already made a list of DNA adducts, including *m/z* [M + H] values of precursor and daughter ions corresponding to more than 250 literature-based DNA

adducts (see additional file 3). Moreover, the data obtained from *in vitro* model reactions such as oxidative stress, inflammation and alkylation are also included in this list. To clarify the mechanisms involved in genotoxicity induced by MGT, here, we examined the comprehensive DNA adduct analysis (DNA adductome analysis) of mice lungs exposed to MGT.

2. Results and Discussion

2.1. Comprehensive Analysis of DNA Adducts Induced by MGT (Nanosized-Magnetite) Treatment

Recently, we have reported that MGT clearly demonstrated genotoxicity in the lungs of *gpt* delta transgenic mice after intratracheal instillation [16]. As a result of mutation spectra analysis, most mutations induced by MGT occurred at G:C base pairs, and the prominent mutation types were a G:C to A:T transition followed by a G:C to T:A transversion [16].

To investigate mechanisms of the induction of mutations in mouse lungs by MGT exposure, we performed comprehensive analysis of DNA adducts according to the methods described in "Experimental Section". Totally, 30 and 42 types of DNA adducts were detected in the vehicle control and MGT-treated groups, respectively (Figure 1, and Additional File 1). Among them, 27 types of adducts were specific for the MGT-treated group, whereas 15 types of adducts overlapped between the MGT-treated and control groups.

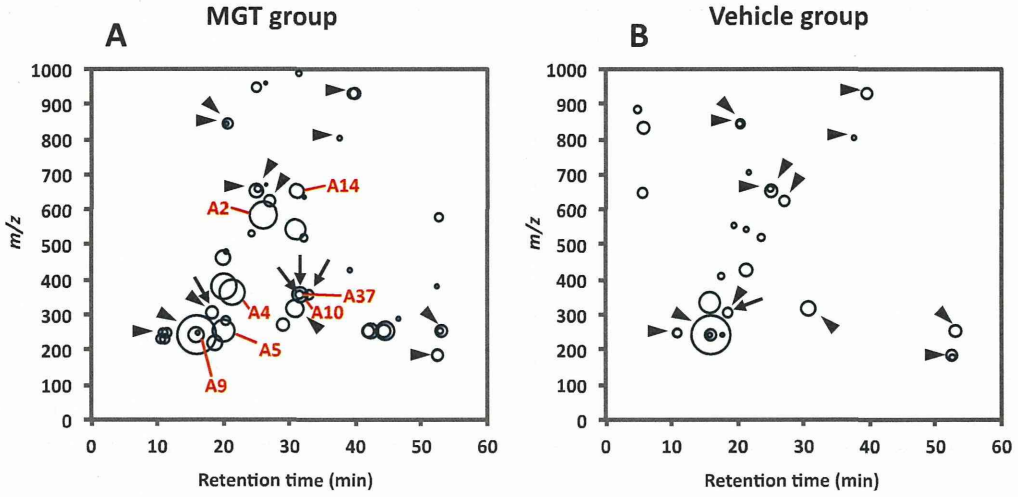

Figure 1. Comprehensive DNA adducts analysis. Map views of DNA adducts in lungs of mice with (**A**) or without MGT-exposure (**B**). Arrow heads indicate the DNA adducts observed in both MGT and vehicle groups, and arrows indicate the corresponding DNA adducts observed in *in vitro* model reactions, including oxidized arachidonic acid, oxidized linoleic acid or hydroxy radical with ctDNA (see additional files 1 and 3). The 7 major contributors determined by PCA and RF analyses are indicated by A2, A4, A5, A9, A10, A14 and A37, respectively.

Principal component analysis (PCA) against a subset of DNA adducts observed in these data set was further applied and is shown in the 2D PCA scores plot (Figure 2A) and associated loadings plot (Figure 2B). A clear clustering of the data could be visualized according to vehicle control and

MGT-treated mice (Figure 2A). The DNA adduct named A5 (*m/z* 252.11 [M + H] at t_R 20.1 min) had the highest contribution to MGT exposure based on its PCA significance. This was followed by DNA adducts named A4 (*m/z* 363.17 [M + H] at t_R 25.9 min), A10 (*m/z* 355.23 [M + H] at t_R 31.0 min), A14 (*m/z* 652.37 [M + H] at t_R 21.4 min) and A9 (*m/z* 243.12 [M + H] at t_R 31.0 min) revealed higher contribution to MGT exposure (Figure 2B). On the other hand, the DNA adduct named A1 demonstrated the highest contribution to the vehicle control. To confirm the results from PCA analysis, a random forest (RF) analysis of the DNA adductome profile data was also performed. The DNA adducts effectively separated the groups (vehicle *vs.* MGT) and are shown in the importance plot (Additional File 1). Several DNA adducts, including A5, A10 and A14, were the most important variables causing the clustering in both mean decrease in accuracy and mean decrease in Gini index (Additional File 1). A hierarchical clustering was analyzed on the dataset consisting of the DNA adducts diagnosed as highly contributing to MGT exposure, including A5 and A10, which were selected from both PCA and RF analyses. As shown in Figure 3, the heatmap for all contributors showed a clear separation of the MGT-treated group from the vehicle control. Among these, A5 was highly correlated with MGT treatment, whereas other contributors, such as A9, A14, A10, A2 and A4 seemed to not always correlate with MGT status. On the other hand, A37 also demonstrated a clear relation with MGT status, however the abundance was lower than that of A5.

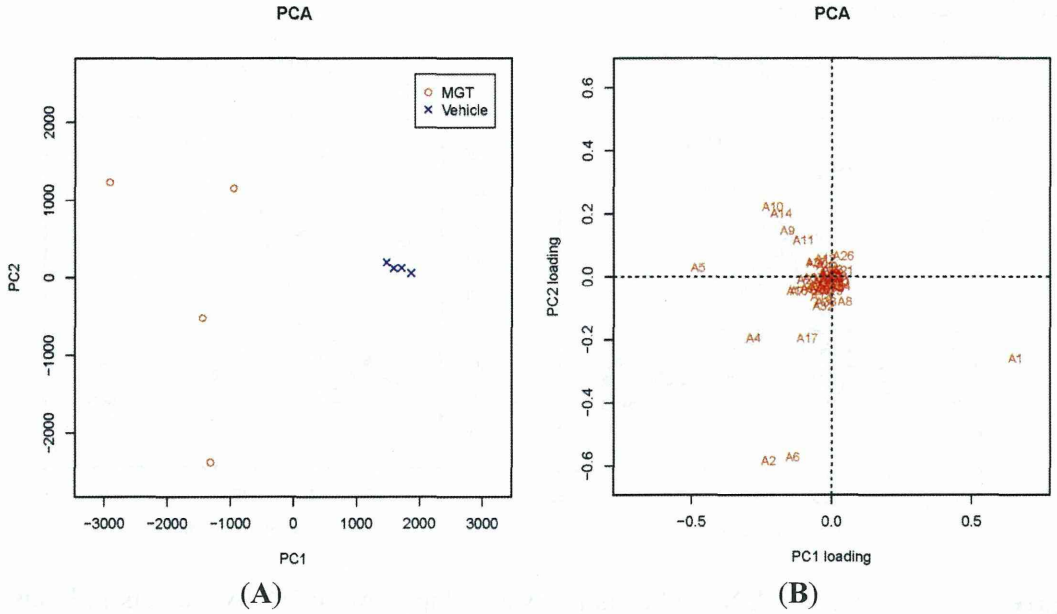

Figure 2. PCA scores and loading plots. (**A**) 2D PCA scores of DNA adducts obtained from adductome analysis. Principal components PC1 and PC2, which explains 74.25% of the total variance observed, discriminate the MGT-treated group from the vehicle control; (**B**) The PC1 and PC2 variable loading plots. Numbers A1–A53 represents DNA adducts observed in DNA adductome analysis.

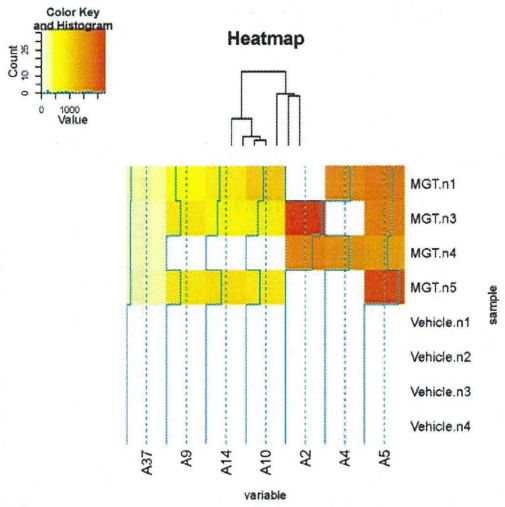

Figure 3. Heatmaps and clustering dendrogram. Hierarchical clustering was performed using 7 major contributors selected by PCA and RF analyses.

2.2. Identification of DNA Adducts Correlated with MGT Treatment

To identify the chemical structure of DNA adducts detected as the "major contributors" to MGT status, we used the list of DNA adducts constructed by ourselves (Additional File 3). Firstly their values of *m/z* [M + H] were compared with known DNA adducts listed in Additional File 3. Among seven major contributors, A4, A5 and A9 indicated identical *m/z* values [M + H] for inflammation-related adducts, ammonium added butano-etheno-deoxyadenosine (BεdA-NH_3, *m/z* 363.1816 [M + H]), etheno-deoxycytidine (εdC, *m/z* 252.0984 [M + H]) and 3-methyldeoxycytidine (3-medC, *m/z* 243.1213 [M + H]), respectively. In contrast to this, we could not find identical *m/z* values [M + H] for the remaining 4 contributors in the DNA adduct list. In order to clarify the formation mechanism of the remaining 4 contributors, A2, A10, A14 and A37, we prepared various *in vitro* model reactions, including oxidative stress and inflammation, and compared their *m/z* values [M + H] and t_R with each other. As a result, A10 (*m/z* 355.23 [M + H] at t_R 31.5 min) and A37 (*m/z* 356.24 [M + H] at t_R 31.4 min) were seen to correspond to one of the DNA adducts observed in the reaction mixture with oxidized-arachidonic acid (Additional Files 1 and 2). No adducts having *m/z* 580.79 [M + H] at t_R 25.9 min (A2) and *m/z* 652.37 [M + H] at t_R 31.0 min (A14) could be seen in any of the *in vitro* model reactions. From these observations, it is suggested that inflammatory responses might exist in the mechanisms behind the increase in mutations by MGT treatment.

2.3. Confirmation of DNA Adducts Correlated with MGT Treatment

In order to confirm the chemical structure of DNA adducts diagnosed as highly contributing to MGT status, we synthesized authentic 15N-εdC and analyzed it by quantitative LC-MS/MS apparatus (Waters 2795 LC system interfaced with a Quattro Ultima triple stage quadrupole MS, (Waters, Manchester, UK)). A peak with a 252.1 ≥ 136.1 transition corresponding to εdC, eluted at the same position as authentic 15N-εdC (255.1 ≥ 139.1), was observed in the lungs of both vehicle and MGT-treated mice (Figure 4). Levels of εdC were significantly higher in the MGT-treated group than those of the vehicle control (Figure 4).

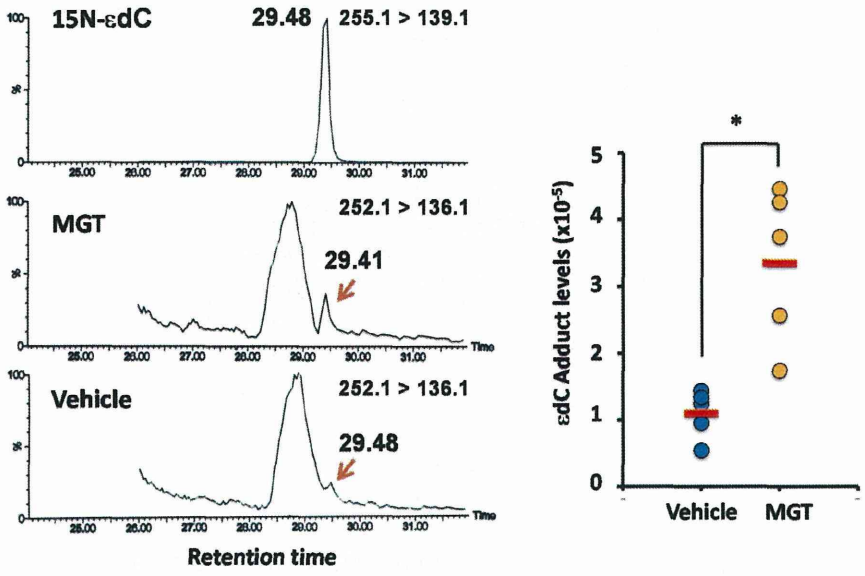

Figure 4. Quantitative Analysis of εdC by LC-MS/MS. εdC formation was induced by MGT exposure in the lungs of ICR mice. DNA was extracted from the lungs 24 h after intratracheal instillation of 0.2 mg per animal of MGT, and was digested enzymatically. Control samples were obtained from the lungs of mice given the vehicle for the same durations of MGT exposure. εdC were quantified by stable isotope dilution liquid chromatography-mass spectrometry (LC-MS/MS). Asterisk (*) indicates a significant difference ($p < 0.05$) from vehicle control (treatment with 0.05% (*v*/*v*) Tween-80) in the Student's *t*-test.

εdC is produced from 4-hydroperoxy-2-nonenal via lipid peroxidation, and is known to be an inflammation-related adduct [22]. Since it has been reported that εdC is involved in C to T transitions using *in vitro* assay [23], it is likely that inflammatory responses might exist in the mechanisms behind the increase in mutations by MGT treatment. Although no data are available regarding the pulmonary inflammation generated by MGT single dose exposure in the present study, we have previously demonstrated that increasing oxidative stress and inflammation-related DNA adducts, including 8-oxodG and HεdC in the lungs of MGT-treated mice [16]. In addition, ROS production and overexpression of heme oxygenase-1, which mediates an anti-inflammatory effect, were clearly observed in MGT-exposed human lung epithelial cells, A549 [14]. Supporting our hypothesis, Park *et al.* [26], have been reported that single intratracheal instillation of magnetite increased the concentration of pro-inflammatory cytokines, such as TNF-α and IL-6, in the cells of bronchoalveolar lavage (BAL) fluid after 24 h exposure. Therefore, in the present study, it is reasonable to consider that inflammatory response evoked from the host reaction against foreign bodies, MGT, induce formation of inflammation-related DNA adducts, such as εdC and HεdC, which, being involved in C to T transitions, are more likely to contribute to genotoxicity observed in the lungs of MGT-exposed mice. Recently, several reports show that the mechanisms of (geno)toxicity induced by nanoparticles are suggested to be involved in macrophage stimulation [26–33]. Innate immune activation through Nalp3 inflammasomes has been suggested to play an important role in the pulmonary inflammation and fibrotic disorders of silicosis and asbestosis [31,32]. He *et al.* [29], demonstrated that multi walled

carbon nanotubes (MWCNTs) directly induce inflammatory cytokines and chemokines, including TNF-α, IL-1β, IL-6, and MCP1 in murine macrophage cell line RAW264.7. Therefore, it is suggested that MGT can activate alveolar macrophage in the same way, then damage adjacent alveolar epithelial cells via cytokine and chemokine activation. In contrast, it has not been ruled out that direct toxicity against alveolar cells might be partly involved in induction of *in vivo* genotoxicity. It has been reported that MWCNTs damaged mitochondria to increase ROS production and cause toxicity against lung alveolar epithelial cells, A549 [29]. Similarly, we also have recently reported that MGT actually manifests cytotoxicity and clastogenicity in cultured mammalian cells [14,15]. Taken together, MGT elicits multiple events such as oxidative stress and inflammatory cytokine production, then leads to genotoxicity in mice lungs.

3. Experimental Section

3.1. Materials

MGT was purchased from Toda Industrial Co., Ltd. (Hiroshima, Japan), and this material was identical to those used in the *gpt* delta mouse study of Totsuka *et al.*, 2014 [16]. The declared primary particle size of MGT was 10.0 nm diameter around. The surface area was 125 m^2/g (disclosed by Toda Industrial Co., Ltd.). Detailed information, such as particle appearance, dispersed diameter and zeta potential of MGT can be found in the previous report [16].

3.2. Chemicals

NucleaseP1 and HPLC grade methanol were purchased from Wako (Tokyo, Japan). Phosphodiesterase I was purchased from Worthington. Bovine spleen phosphodiesterase II, DNase I, Type I agarose, low melting point agarose, and Triton X-100 and bacterial alkaline phosphatase Type III (*E. coli*) were purchased from Sigma Co. (St. Louis, MO, USA). All other chemicals used were of analytical grade and purchased from Wako.

3.3. Animals

Male ICR mice (6 weeks old) were obtained from Japan SLC (Shizuoka, Japan). Animals were provided with food (CE-2 pellet diet, CLEA Japan, Inc., Tokyo, Japan) and tap water *ad libitum* and quarantined for one week. Mice were maintained under controlled conditions: 12 h light/dark cycle, 22 ± 2 °C room temperature, and 55% ± 10% relative humidity. The experiments were conducted according to the "Guidelines for Animal Experiments in the National Cancer Center" of the Committee for Ethics of Animal Experimentation of the National Cancer Center.

3.4. Analysis of DNA Adducts

For DNA adduct analyses, each group of 4 to 5 male ICR mice was intratracheally instilled with MGT at a single dose of 0.2 mg per animal, and sacrificed 24 h after MGT administration. Our previous study [16] demonstrated that *gpt* mutation frequency was significantly increased in mice lungs treated with multiple doses of 0.2 mg, but not in the 0.05 mg treatment group. In the DNA

adduct formation analysis, even though singly treated with 0.2 mg of MGT, the levels of oxidative stress related DNA adducts were significantly increased. Therefore, we thought that a single dose of 0.2 mg MGT/animal was sufficient to analyze comprehensive DNA adduct analysis. Control samples were obtained from the lungs of mice given the vehicle. Mouse lung DNA was extracted and purified using a Gentra® Puregene™ tissue kit (QIAGEN, Valencia, CA, USA). The protocol was performed according to the manufacturer's instructions except that desferroxamine (final concentration: 0.1 mM) was added to all solutions to avoid the formation of oxidative adducts during the purification step. The extracted DNA was stored at −80 °C until analysis for DNA adductome analysis.

3.4.1. Comprehensive Analysis of DNA Adducts (DNA Adductome Analysis)

Mouse lung DNA extracted from vehicle (n = 4) and MGT treated (n = 4) mice were enzymatically digested according to the method of Goodenough *et al.* [24], with some modifications. Briefly, internal standards (2',3'-dideoxyinosine and 2',3'-dideoxyguanosine) were added to the DNA solution prior to enzyme digestion, at 12.7 nM. The enzymatic digestion conditions are as follows; DNA (67 μg) in 5 mM Tris-HCl buffer (pH 7.4) employed DNase I (Type IV from bovine pancreas) for 3 h. Next, nuclease P1 (from *Penicillium citrinum*), 10 mM sodium acetate (pH 5.3, final 10 mM), and $ZnCl_2$ (final 34 mM) were added, and incubated for a further 3 h at 37 °C. Alkaline phosphatase (from *E. coli*), phosphodiesterase I (20 U/mL in water) and Tris base (final 15.4 mM) were added last, for an additional 16–18 h at 37 °C. The sample was purified using Vivacon500® (10 kDa molecular weight cut-off filters, Sartorius AG, Goettingen, Germany), then, the reaction mixture was centrifuged (4 °C, 10,000× *g*, 15 min) using Ultrafree® (0.2 μm pore; Millipore Co., Billerica, MA, USA) and the filtrate was used for DNA adductome analysis.

LC-MS analyses were performed using a nanoACQUITY UPLC system (Waters, Milford, MA, USA) equipped with a Xevo QTOF mass spectrometer (Waters, Manchester, UK), instrumented with an electrospray ionization source (ESI) and controlled by MassLynx 4.1 software. Sample injection volumes of 4 μL each were separated on a ACQUITY UPLC BEH130 C18 column (1.7 μm, 1.0 mm i.d. × 150 mm) at a flow rate of 25 μL/min. The column temperature was set to 40 °C. Mobile phase A and B were water and methanol, respectively. Chromatographic separation was performed by a gradient elution as follows: 0–5 min, 1% B; 5–10 min, linear gradient to 10% B; 10–35 min, linear gradient to 80% B; 35–45 min, 80% B. MS parameters were set as follows: mass range scanned from 50 to 1000 with a scan duration of 0.5 s (1.0 s total duty cycle), capillary 3.7 kV, sampling cone 40 V, extraction cone 4 V, source temperature 125 °C, desolvation temperature 250 °C. Nitrogen gas was also used as the desolvation gas (flow 800 L/h) and cone gas (30 L/h). All data were collected in positive ion mode. MS^E analysis was performed on the mass spectrometer set at 3 V for low collision energy and ramp of 10–25 V for high collision energy during the acquisition cycle. A cone voltage of 20 V was used. LockMass parameters were set as following: capillary 3.0 kV, sample cone 40 V, collision energy 21 V.

Relative peak intensity of each potential DNA adduct was calculated as previously described [33]. The relative peak intensity was plotted as a bubble chart in which the horizontal axis was retention time and the vertical axis was *m/z*. DNA obtained from normal human fetal fibroblast cell line, TIG-3, with internal standard was used as a reference [33].

3.4.2. Data Processing

The raw data files obtained from LC/MS runs were analyzed using MassLynx v4.1 and MarkerLynx 4.1 software (Waters). The application detects, integrates, and normalizes the intensities of the peaks to the sum of peaks within the sample. The resulting multivariate dataset consisting of the peak number (based on the retention time and *m/z*), sample name, and the normalized peak intensity was analyzed by S-plot analysis using SIMCA-P+ 11.5 (Umetrics AB, Umea, Sweden). The method parameters were as follows: Mass tolerance = 0.05 Da, Apex Track Parameters: Peak width at 5% height (seconds) = 15/Peak-to-peak baseline noise = 50, Apply smoothing = Yes, Collection Parameters: Intensity threshold (counts) = 100/Mass window = 0.05/Retention time window = 0.10, Noise elimination level = 6, Deisotope data = Yes.

3.4.3. *In Vitro* Modification of DNA

The DNA modification derived from oxidation of unsaturated fatty acids was performed by incubating calf thymus DNA (ctDNA, 1 mg/mL, Sigma, Steinheim, Germany) with 20 mM unsaturated fatty acids including arachidonic acid (Sigma) and linoleic acid (Sigma) in the presence of 75 μM $CuSO_4$ (Wako) and 1.5 mM ascorbic acid (Wako). The DNA modification related to oxidative stress was formed from ctDNA and 10 mM hydrogen peroxide (Wako) in the presence of 1 mM $CuSO_4$ and 1 mM ascorbic acid in 1 mL of 500 mM sodium phosphate buffer, pH 7.4 for 24 h, in atmospheric oxygen at 37 °C. The reaction was terminated by the addition of 1 mM butylated hydroxytoluene (Wako) and 100 μM diethylenetriaminepentaacetic acid (Wako).

3.4.4. Confirmation of εdC

Mouse lung DNA (40 μg) extracted from vehicle (n = 5) and MGT treated (n = 5) mice was enzymatically digested, and εdC was analyzed and quantified by the Waters 2795 LC system (Waters, Manchester, UK) interfaced with a Quattro Ultima triple stage quadrupole MS (Waters) using the same procedure previously described [34]. Authentic 15N-εdC was kindly provided by Dr. Yoshitaka Matsushima (Tokyo University of Agriculture) synthesized according to previously published methods [35]. The multiple reaction monitoring transitions were monitored; each cone voltage and collision energy used were εdC [252.1 ≥ 136.1, 35 V, 10 eV].

3.5. Statistical Analysis

PCA and RF analyses were used for modeling comprehensive analysis of DNA adducts (DNA adductome analysis). All the calculations were performed using statistical package R. In RF, we confirmed that the out-of-bag misclassification rate was saturated at 0% with 100,000 generated trees with two variables. The data were statistically compared with the corresponding solvent control using the Student's t test for DNA adduct formation. The data were compared with the corresponding solvent control using the F test before application of the Student's t test. If the F test evaluation showed an unequal variance, the p value was determined using the Welch's t test.

4. Conclusions

We have demonstrated that MGTs induce inflammation-related DNA adduct formation in mouse lungs by using comprehensive analysis of DNA adducts, DNA adductome analysis. In PCA analysis, εdC was detected as the "major contributor" to MGT status. Due to the inducible base, the exchange pattern of εdC has been reported to be a C to T transition [22.23], being the predominant mutational pattern detected in mouse lungs exposed to MGT [16]. Therefore, it is suggested that inflammatory responses lead to inflammation-related DNA adduct formations, such as εdC, and this might contribute to the genotoxicity in mouse lungs induced by MGT treatment.

Acknowledgments

We thank Naoaki Uchiya, Yoko Matsumoto and Akihiro Sekine for their excellent technical assistance. This study was supported by Grants-in-Aid for Cancer Research, for the U.S.-Japan Cooperative Medical Science Program, for Research on Risk of Chemical Substances from the Ministry of Health, Labor, and Welfare of Japan, for Young Scientists (B) 23710084 from the Ministry of Education, Culture, Sports, Science and Technology of Japan. The study was also supported by a grant from the Japan Chemical Industry Association (JCIA) Long-range Research Initiative (LRI). Kousuke Ishino was the recipient of a Research Resident Fellowship from the Foundation for Promotion of Cancer Research.

Author Contributions

Kousuke Ishino, Yukari Totsuka and Tatsuya Kato performed DNA adducts analysis and drafted the manuscript. Mamoru Kato carried out statistical analysis. Analysis of size distribution and agglomeration state of particles were done by Masatoshi Watanabe. Tatsuhiro Shibata, Keiji Wakabayashi and Hitoshi Nakagama conceived and supervised the study. All authors read and approved the final manuscript.

Appendix

Additional File 1. List of the data set obtained from DNA adductome analysis.

Peak No.	RT (min)	*m/z*	Area Mean ± SD		*p*-Value (*t* Test)	Fold Change
			MGT	Vehicle		
1	16.0	242.11	4867 ± 722	4938 ± 2414	0.485	0.99
2	25.9	580.79	2389 ± 837	-	-	-
3	21.4	363.17	2016 ± 850	-	-	-
4	20.1	252.11	1543 ± 375	-	-	-
5	31.0	543.33	1273 ± 732	-	-	-
6	44.4	252.11	1099 ± 669	-	-	-
7	30.9	317.17	957 ± 125	676 ± 363	0.294	1.41
8	16.0	243.12	775 ± 112	-	-	-
9 [a]	31.5	355.23	758 ± 221	-	-	-

Additional File 1. *Cont.*

Peak No.	RT (min)	*m/z*	Area Mean ± SD		*p*-Value (*t* Test)	Fold Change
			MGT	Vehicle		
10	18.8	219.11	703 ± 819	-	-	-
11	20.0	463.73	677 ± 504	-	-	-
12	31.0	652.37	632 ± 249	-	-	-
13	25.0	655.40	591 ± 188	493 ± 39	0.106	1.20
14	28.9	273.18	491 ± 205	-	-	-
15	41.8	252.11	471 ± 111	-	-	-
16 [c]	18.4	308.13	468 ± 129	293 ± 27	0.010	1.59
17	53.0	252.11	458 ± 182	455 ± 162	0.447	1.03
18	52.5	181.98	415 ± 167	387 ± 156	0.425	1.07
19	26.9	622.79	411 ± 132	349 ± 110	0.287	1.18
20	39.7	928.61	379 ± 137	384 ± 83	0.490	0.99
21	20.2	841.27	317 ± 310	259 ± 179	0.452	1.23
22	11.0	230.11	295 ± 82	-	-	-
23 [b]	32.9	360.21	269 ± 98	-	-	-
24	25.0	946.44	265 ± 154	-	-	-
25	20.2	284.13	252 ± 34	-	-	-
26	10.9	250.08	252 ± 70	264 ± 135	0.176	0.95
27	52.5	575.30	213 ± 49	-	-	-
28 [a]	31.4	356.24	207 ± 50	-	-	-
29	32.0	517.69	174 ± 79	-	-	-
30	25.0	656.40	136 ± 33	115 ± 11	0.393	1.19
31	24.2	530.75	117 ± 38	-	-	-
32	52.8	253.11	108 ± 83	-	-	-
33	31.4	988.64	98 ± 23	-	-	-
34	37.5	800.44	70 ± 27	61 ± 13	0.451	1.14
35	39.1	429.25	58 ± 10	-	-	-
36	16.0	245.23	53 ± 27	-	-	-
37	52.4	382.20	50 ± 10	-	-	-
38	20.4	842.28	47 ± 41	123 ± 56	0.367	0.38
39	32.1	633.74	33 ± 25	-	-	-
40	32.1	634.10	33 ± 4	-	-	-
41	26.3	961.47	26 ± 14	-	-	-
42	26.4	667.80	19 ± 9	-	-	-

[a] This peak overlapped with one of the adducts produced by reaction of oxidized arachidonic acid with ctDNA (data not shown); [b] This peak overlapped with one of the adducts produced by reaction of hydroxy radical with ctDNA (data not shown); [c] This peak overlapped with one of the adducts produced by reaction of oxidized linoleic acid with ctDNA (data not shown).

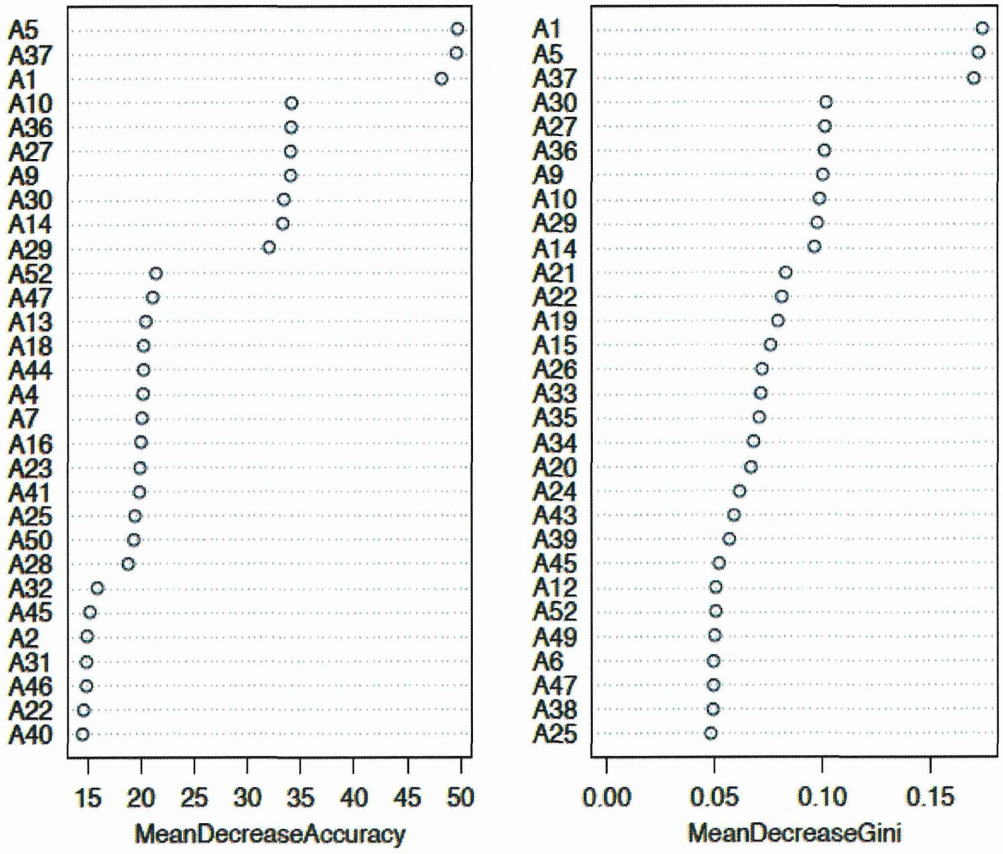

Additional File 2. RF Dotchart of variable importance for vehicle control *vs.* MGT-treated group.

Additional File 3. Information of the authentic DNA adducts.

Adduct	Precurser (M + H)	Product (Deoxyribose Loss)	Ref.	Na 22.9898	K 39.0983	NH_3 18.0379
5-MedC	242.1140	126.0666	-	264.0960	280.2045	259.1441
dU	229.0824	113.0350	[36]	251.0644	267.1729	246.1125
dI	253.0936	137.0462	[36]	275.0756	291.1841	270.1237
dX	269.0886	153.0412	[36]	291.0706	307.1791	286.1187
dO	269.0886	153.0412	[36]	291.0706	307.1791	286.1187
8-Oxo-dG	284.0994	168.0520	[37]	306.0814	322.1899	301.1295
Sp	300.0944	184.0470	[38]	322.0764	338.1849	317.1245
Gh	274.1151	158.0677	[38]	296.0971	312.2056	291.1452
Iz	229.0937	113.0463	[38]	251.0757	267.1842	246.1238
Oz	247.1042	131.0568	[39]	269.0862	285.1947	264.1343
FapyG	286.1151	170.0677	[39]	308.0971	324.2056	303.1452
Oxa	249.0723	133.0249	[38]	271.0543	287.1628	266.1024
Cyclo-dG	266.0889	150.0415	[40]	288.0709	304.1794	283.1190
Cyanuric acid	246.0726	130.0252	[38]	268.0546	284.1631	263.1027
CAC	288.0944	172.0470	[41]	310.0764	326.1849	305.1245
HICA	277.0672	161.0198	[41]	299.0492	315.1577	294.0973
8-OH-dA	268.1046	152.0572	[39]	290.0866	306.1951	285.1347

Additional File 3. *Cont.*

Adduct	Precurser (M + H)	Product (Deoxyribose Loss)	Ref.	Na 22.9898	K 39.0983	NH_3 18.0379
2-OH-dA	268.1046	152.0572	[42]	290.0866	306.1951	285.1347
FapydA	270.1202	154.0728	[39]	292.1022	308.2107	287.1503
Cyclo-dA	250.0940	134.0466	[39]	272.0760	288.1845	267.1241
5-OHdC	244.0933	128.0459	[39]	266.0753	282.1838	261.1234
5-HmdU	259.0930	143.0456	[39]	281.0750	297.1835	276.1231
FodU	257.0773	141.0299	[39]	279.0593	295.1678	274.1074
Tg	277.1036	161.0562	[39]	299.0856	315.1941	294.1337
d(G[8–5]C)	555.1353	439.0879	[43]	515.1615	531.2700	510.2096
d(G[8–3]T)	508.1792	392.1318	[44]	530.1612	546.2697	525.2093
d(G[8–5m]T)	508.1792	392.1318	[45]	530.1612	546.2697	525.2093
εdA	276.1096	160.0622	[39]	298.0916	314.2001	293.1397
εdC	252.0984	136.0510	[39]	274.0804	290.1889	269.1285
ε5mdC	266.1100	150.0626	[46]	288.0920	304.2005	283.1401
εdG	292.1046	176.0572	[39]	314.0866	330.1951	309.1347
M1dG	304.1046	188.0572	[39]	326.0866	342.1951	321.1347
5,6-dihydro-M1dG	306.1202	190.0728	[47]	328.1022	344.2107	323.1503
PdG	308.1359	192.0885	[39]	330.1179	346.2264	325.1660
6-oxo-M1dG	320.0995	204.0521	[48]	342.0815	358.1900	337.1296
MDA-dA	306.1202	190.0728	[49]	328.1022	344.2107	323.1503
MDA-dC	282.1090	166.0616	[49]	304.0910	320.1995	299.1391
8-OH-PdG	324.1307	208.0833	[50]	346.1127	362.2212	341.1608
6-OH-PdG	324.1307	208.0833	[50]	346.1127	362.2212	341.1608
propano-dA	308.1359	192.0885	[51]	330.1179	346.2264	325.1660
propano-dC	286.1403	170.0929	[51] *	308.1223	324.2308	303.1704
propano-5MedC	300.1560	184.1086	[51] *	322.1380	338.2465	317.1861
FDP-dG	362.1465	246.0991	[52] *	384.1285	400.2370	379.1766
α-Me-γ-OH-PdG (R- or S-α-Me-γ-OH-CRA-dG)	338.1464	222.0990	[50]	360.1284	376.2369	355.1765
Croton-dA	322.1516	206.1042	[50] *	344.1336	360.2421	339.1817
Croton-dC	300.1560	184.1086	[50] *	322.1380	338.2465	317.1861
Croton-5MedC	314.1717	198.1243	[50] *	336.1537	352.2622	331.2018
ICL-RD	589.2483	473.2009	[53]	611.2303	627.3388	606.2784
ICL-R	587.2326	471.1852	[53]	609.2146	625.3231	604.2627
ICL-S	587.2326	471.1852	[53]	609.2146	625.3231	604.2627
Hexanoyl-dG	366.1777	250.1303	[54] *	388.1597	404.2682	383.2078
Hexenal-dG	366.1777	250.1303	[55]	388.1597	404.2682	383.2078
HNE-dG	424.2196	308.1722	[56]	446.2016	462.3101	441.2497
HNE-dA	408.2248	292.1774	[56] *	430.2068	446.3153	425.2549
HNE-dC	386.2292	270.1818	[56] *	408.2112	424.3197	403.2593
HNE-5MedC	400.2449	284.1975	[56] *	422.2269	438.3354	417.2750
HεdG	404.1933	288.1459	[57]	426.1753	442.2838	421.2234

Additional File 3. *Cont.*

Adduct	Precurser (M + H)	Product (Deoxyribose Loss)	Ref.	Na 22.9898	K 39.0983	NH_3 18.0379
HεdA	388.1984	272.1510	[57]	410.1804	426.2889	405.2285
HεdC	364.1872	248.1398	[57]	386.1692	402.2777	381.2173
HεMedC	378.2029	262.1555	[57] *	400.1849	416.2934	395.2330
BεdG	362.1464	246.0990	[58]	384.1284	400.2369	379.1765
BεdA	346.1515	230.1041	[58] *	368.1335	384.2420	363.1816
BεdC	322.1402	206.0928	[58]	344.1222	360.2307	339.1703
BεMedC	336.1559	220.1085	[58]	358.1379	374.2464	353.1860
CHPdG	460.2196	344.1722	[59] *	482.2016	498.3101	477.2497
CHPdA	444.2247	328.1773	[59] *	466.2067	482.3152	461.2548
CHPdC	420.2134	304.1660	[59] *	442.1954	458.3039	437.2435
CPPdG	404.1570	288.1096	[59] *	426.1390	442.2475	421.1871
CPPdA	388.1621	272.1147	[59] *	410.1441	426.2526	405.1922
CPPdC	364.1508	248.1034	[59] *	386.1328	402.2413	381.1809
CEPdG	390.1413	274.0939	[59] *	412.1233	428.2318	407.1714
CEPdA	374.1464	258.0990	[59] *	396.1284	412.2369	391.1765
CEPdC	350.1352	234.0878	[59] *	372.1172	388.2257	367.1653
N^6-HmdA	282.1202	166.0728	[60]	304.1022	320.2107	299.1503
N^6-MedA	266.1253	150.0779	[61]	288.1073	304.2158	283.1554
N^2-Ethylidene-dG	294.1202	178.0728	[62]	316.1022	332.2107	311.1503
N^2-ethyl-dG	296.1359	180.0885	[62]	318.1179	334.2264	313.1660
1-medA	268.1409	152.0935	[38]	290.1229	306.2314	285.1710
3-medC	243.1213	127.0739	[38]	265.1033	281.2118	260.1514
N^2-CMdG	326.1100	210.0626	[63]	348.0920	364.2005	343.1401
Glyoxal-dA	310.1152	194.0678	[63]	332.0972	348.2057	327.1453
Glyoxal-dC	288.1196	172.0722	[63]	310.1016	326.2101	305.1497
Glyoxal-5MedC	302.1353	186.0879	[63] *	324.1173	340.2258	319.1654
N^2-CEdG	340.1257	224.0783	[64]	362.1077	378.2162	357.1558
8-Cl-dG	302.0656	186.01824	[65]	324.0476	340.1561	319.0957
8-Cl-dA	286.0707	170.02334	[65]	308.0527	324.1612	303.1008
5-Cl-dC	262.0594	146.01204	[65]	284.0414	300.1499	279.0895
8-Br-dG	346.0151	229.96774	[66]	367.9971	384.1056	363.0452
8-Br-dA	330.0202	213.97284	[66] *	352.0022	368.1107	347.0503
5-Br-dC	306.0089	189.96154	[67]	327.9909	344.0994	323.039

Na: sodium added form; K: potassium added form; NH_3: ammonium added form; *: Expected *m/z* calculated by Symyx Draw 4.0 software (Accelrys Inc., San Diego, CA, USA).

Conflicts of Interest

The authors declare no conflict of interest.

References

1. Cabreraa, L.; Gutierreza, S.; Menendezb, N.; Moralesc, M.P.; Herrasti, P. Magnetite nanoparticles: Electrochemical synthesis and characterization. *Electrochim. Acta* **2008**, *53*, 3436–3441.